NANO LETTERS

pubs.acs.org/NanoLett

Mini Review

I–III–VI Quantum Dots and Derivatives: Design, Synthesis, and Properties for Light-Emitting Diodes

Linxiang Yang,[⊥] Shuai Zhang,*[,⊥] Bo Xu, Jiangyuan Jiang, Bo Cai, Xinyi Lv, Yousheng Zou, Zhiyong Fan, Heesun Yang,* and Haibo Zeng*

Cite This: https://doi.org/10.1021/acs.nanolett.2c03138

Read Online

ACCESS | Metrics & More | Article Recommendations

ABSTRACT: Quantum dots (QDs) are important frontier luminescent materials for future technology in flexible ultrahigh-definition display, optical information internet, and bioimaging due to their outstanding luminescence efficiency and high color purity. I–III–VI QDs and derivatives demonstrate characteristics of composition-dependent band gap, full visible light coverage, high efficiency, excellent stability, and nontoxicity, and hence are expected to be ideal candidates for environmentally friendly materials replacing traditional Cd and Pb-based QDs. In particular, their compositional flexibility is highly conducive to precise control energy band structure and microstructure. Furthermore, the quantum dot light-emitting diodes (QLEDs) exhibits superior prospects in monochrome display and white illumination. This review summarizes the recent progress of I–III–VI QDs and their application in LEDs. First, the luminescence mechanism is illustrated based on their electronic-band structural characteristics. Second, focusing on the latest progress of I–III–VI QDs, the preparation mechanism, and the regulation of photophysical properties, the corresponding application progress particularly in light-emitting diodes is summarized as well. Finally, we provide perspectives on the overall current status and challenges propose performance improvement strategies in promoting the evolution of QDs and QLEDs, indicating the future directions in this field.

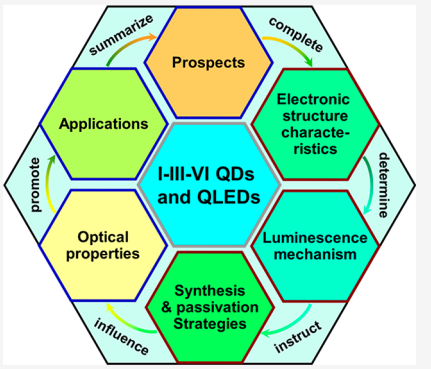

KEYWORDS: *I–III–VI, quantum dots, photoelectric characteristic, photophysical mechanism, light-emitting diodes*

INTRODUCTION

Light-emitting diodes (LEDs) are the key equipment of human–computer interaction and human–thing interconnection. Future display technology not only has a trillion magnitude of economic scale but also reflects the national regional innovation ability and cutting-edge technology competitiveness. Especially ultrapure color luminescent quantum dots (QDs) are the key materials of high-definition (HD), flexible, and intelligent LEDs. Relatively mature QD systems for new-generation LEDs such as II–VI (e.g., CdSe, PbS), III–V (e.g., InP), and perovskite QDs, have tackled the bottlenecks of efficiency and lifetime.[1−4]

I–III–VI QDs and derivatives exhibit excellent prospects in candidates for future high-quality electronic devices of solar cells, photocatalysis, biological imaging, and LEDs,[5−11] especially the superior semiconductor properties of direct band gap,[12] tunable band structure, high photoluminescence quantum yield (PLQY), and energy convergence in excited state,[13,14] which are essential factors for QLEDs. This review first summarizes the precise structure design and luminescence mechanism and then generalizes the crucial factors of synthesis; afterward, optical performance and QLEDs are demonstrated in detail. Finally, perspectives on the overall current status, challenges, and improvement strategies in promoting the evolution of QDs and QLEDs are proposed, indicating the future directions in this field.

ELECTRONIC STRUCTURE CHARACTERISTICS

I–III–VI QDs generally exist as chalcopyrite, zinc blende, and wurtzite at room temperature (Figure 1a).[15] Chalcopyrite is characterized by tetragonal crystal system, with monovalent and trivalent elements arranged in order, while elements (I/III) are interchangeable in zinc blende and wurtzite, therefore inevitably introducing defects in crystals. In addition, I–III–VI QDs can coexist in three phases at room temperature,[16] which is one of the reasons why there are many morphologies in QDs colloidal solutions.

In typical I–III–VI QDs, I, III, and VI are Ag^+/Cu^+, Ga^{3+}/In^{3+}, and S^{2-}/Se^{2-} respectively (such as Ag–In–S (AIS),[17] Cu–Ga–S (CGS),[18] Cu–Ga–Se (CGSe)).[6] Introducing homologous or heterogeneous ions (Al^{3+}, Zn^{2+}, Sn^{4+}, Fe^{3+})

Received: August 8, 2022
Revised: March 13, 2023

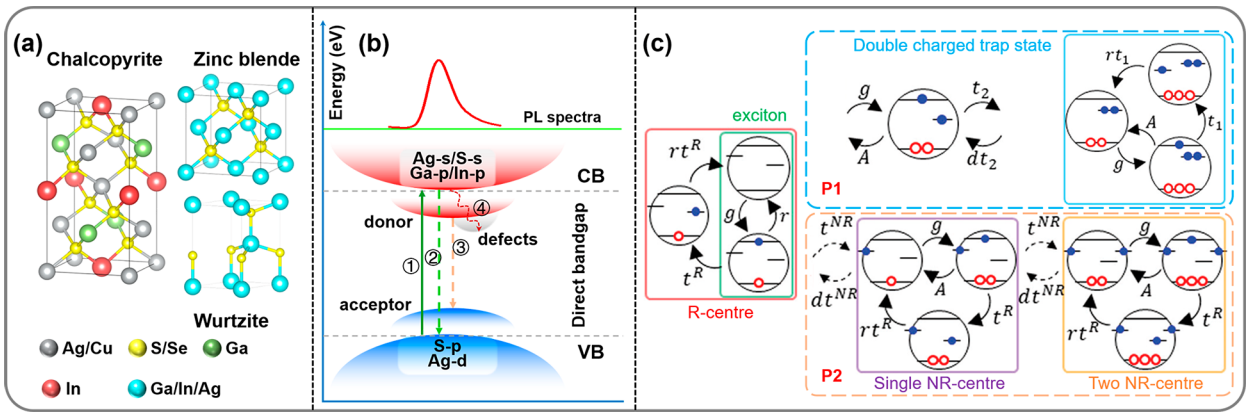

Figure 1. (a) Lattice structure of I−III−VI QDs (chalcopyrite, zinc blende, wurtzite). (b) Electronic band structure of I−III−VI QDs and different paths of recombination or quenching, the tail in the spectra originate from the energy level of donor, acceptor and defects. (c) Schematic diagram of radiative recombination (exciton and double-charge-trap-state recombination) and nonradiative recombination (single- and two-center nonradiative recombination).[28] Adapted with permission from ref 28. Copyright 2022 Royal Society of Chemistry.

can further derive the composition into quaternary/quinary QDs,[19] the main compounds are Ag−In−Ga−S (AIGS),[20−23] Ag−Cu−Ga−Se (ACGSe),[24] Zn−Cu−Ga−S (ZCGS),[25,26] and Zn−Ag−In−Ga−S (ZAIGS).[27]

I−III−VI QDs and derivatives demonstrate flexible chemical composition and nonstoichiometric characteristics, meanwhile the defects can participate in the radiative recombination process. The electronic and structural characteristics of I−III−VI QDs and derivatives can be concluded as follows.

Direct Band Gap. The conduction band minimum (CBM) and valence band maximum (VBM) correspond to the same wave vector, which means that there could be no loss of energy, allowing for the PLQY up to 100%. According to the first-principles calculation for AGS, the CBM and VBM are both at Γ-point, which indicate the properties of direct-band semiconductor of I−III−VI QDs.

Tunable Band Structure. The chemical composition of I−III−VI QDs and derivatives exhibit considerable flexibility and substitutability, which own the merits of full coverage of visible light and finely customized electronic band structure. The larger ions of III (In^{3+}) and VI (S^{2-}, Se^{2-}) can reduce the band gap by tuning the electron band structure and keep the emission of QDs in the red and infrared ranges, which is advantageous for red LEDs, solar cells, photocatalysis, and bioimaging.[27,29−32] For green and blue QDs, smaller ions (Ga^{3+}, Al^{3+}, Bi^{3+} and Zn^{2+}, etc.) are necessary, especially Ga^{3+} and Al^{3+}, which can tune the spectra of QDs to the green and blue ranges with narrower full-width at half maximum (FWHM),[26,33] which expand the applications of LEDs. The Zn^{2+} has been reported to have strong ability in regulating emissive spectra; Tang et al. discovered the extended blueshift in Zn^{2+}-doped AIGS QDs.[26] The ZnS shell also blues shift spectra by limiting excited state energy.[34] In addition, the defects formed by nonstoichiometric show adjustment in emissive spectra of QDs as well, serve as radiative recombination centers. For instance, the defects in $CuAl_5S_8$/ZnS QDs provided a recombination channel from I_{Cu}/Al_{Cu} to V_{Cu}/V_{Al}, leading to the strong emission at 470 nm.[33] Simultaneously, the V_{Cu}-defect density would cause the energy level of defect (acceptor) shift, thus regulating the emission spectra.[35]

The energy structure and emissive spectrum are affected by the size of QDs as well. Quantum confinement effect, which is approximately described by Brus' effective-mass (EMM) model, described how the smaller particle size of QDs make the band gap larger.[36] Takahisa et al. indicated that the PL of AGS/CGS could be blue-shifted from 500 to 400 nm as the particle size decreased from 6 to 2 nm.[37] However, the smaller particle size (2−7 nm) than Bohr radius (4 nm for $CuGaS_2$, 5.5 nm for $AgInS_2$), making it easier for I−III−VI QDs to split into sublevels near the CB and VB,[16,36,38] which tends to result in asymmetric PL broadening and higher defect state density.[39] The tunable emission of I−III−VI QDs also exhibits advantages in terms of broad-emission spectra. The multiple recombination centers can be adjusted by the split sublevels and defect-mediated levels, which contributes to white-emission QDs and single-QDs WLEDs.

Energy Convergence of the Excited State. Because of the flexible chemical composition and defect-related exciton recombination, the emission purity is inevitably severely limited. By precisely designing the structure, the luminescence efficiency and FWHM of the QDs can be improved effectively. Although there is no clear study on the intrinsic mechanism in spectral narrowing, reasonable speculations can be drawn as follows: adjusting the defect band level close to the CBM and VBM and making QDs more tolerant of defect. For example, doping and alloying of Ga^{3+} and Zn^{2+} can effectively fill the defect (V_{In}, In_{Ag}) to eliminate donor/acceptor radiative recombination associated with smaller band gap (V_{In}/In_{Ag} to V_{Ag}/VBM).[11,21]

LUMINESCENCE MECHANISM

Based on the electronic-structure characteristics of I−III−VI QDs and derivatives, the luminescence mechanism should be probed in depth. The band structure of I−III−VI QDs and derivatives are demonstrated in Figure 1b, the I/VI-s and III-p orbital form the CB, while I-d (contribution of s and p are usually ignored) and VI-p orbital constitute the VB.[40] For instance of AGS and CGS, the CBM mainly depends on the hybridization of Ag/Cu s-orbital with Ga p-orbital, while the VBM is dominated by the hybridization of the Ag/Cu d-orbital with the S p-orbital. The band gap of AGS is larger than that of CGS, and the distribution pattern of the CB is more concentrated, which can result from the difference of d-state distribution between Ag and Cu in density of states (DOS). Notably, the hybridization of Cu-compounds at the top of VB

https://doi.org/10.1021/acs.nanolett.2c03138
Nano Lett. XXXX, XXX, XXX−XXX

Table 1. Synthetic Methods and Optical Performance of I−III−VI QDs and Derivatives[a]

QDs	precursors, ligands, solvents	methods	T [°C]	emission [nm]	PLQY [%]	ref.
CIGS/ZnS	CuI, $In(Ac)_3$, $Ga(acac)_3$, $Zn(Ac)_2$, $Zn(St)_2$, ODE, OTT, OA	HI	230−240	479−578	20−85	50
AIGS	$AgNO_3$, $In(Ac)_3$, $Ga(acac)_3$, S, DDT, OAm, ODE, HPA, TDPA, ODPA	HI	120	628		5
ACGS	$AgNO_3$, $Ga(acac)_3$, $Zn(St)_2$, S, DDT, OAm	HU		470−530	2−16.7	26
AIGS/ZnS	AgI, $In(Ac)_3$, $Ga(acac)_3$, S, $ZnCl_2$, $Zn(Ac)_2$, $Zn(St)_2$, ODE, DDT, OAm,	HI	240−250	450−570	58−69	53
AIGS/GaS	Ag(Ac), $In(Ac)_3$, $Ga(DDTC)_3$, $Ga(acac)_3$, DMTU, OAm, TBP	HU	150−280	498−601	28−56	56
AIGS	Ag(Ac), $In(Ac)_3$, $Ga(DDTC)_3$, $Ga(acac)_3$, DMTU, OAm, MX_n	HU	150−280	518	73.4	20
AIS/GaS_x	$AgNO_3$, S, $In(OAc)_3$, $Ga(acac)_3$, DMTU, OAm	HU	30−130, 280	530−660		57
AIGS/GaS	Ag(Ac), $In(Ac)_3$, $Ga(DDTC)_3$, $Ga(acac)_3$, DMTU, OAm,	HU	280	535−543	51.9	47
AIS/GaS	Ag(Ac), $In(Ac)_3$, $Ga(acac)_3$, DMTU, OAm, TOP	HI	140−280	578	72.3	21
ZAIGS	$Ag_xIn_yGa_{2-x-y}Zn_2(S_2CN(C_2H_5)_2)_4$, OAm	HU	190, 220, 250	515−716	14.3−48.3	27
$AgIn_xGa_{1-x}S_2/GaS_y$	$InCl_3$, $In(DDTC)_3$, $Ga(DDTC)_3$, Ag(OAc), OAm	HI	200, 230−280	499−543	60	44
ZCGS: Mn	CuI, GaI_3, DDT, OAm, S, ODE, $Mn(Ac)_2$	HI	190		75−78	58
ZCGSSe	CuI, GaI_3, DDT, OAm, S, Se, $Zn(Ac)_2$, TOP, DPP, ODE, OA	HI	240−260	485−630	73−85	6
ZCGS	CuI, GaI_3, DDT, S, $ZnCl_2$, $Zn(Ac)_2$, $Zn(St)_2$, OAm, ODE, OA	HI	240−250	471−486	78−83	25
AIS/GaS	Ag(Ac), $In(Ac)_3$, TU, ODE, $Ga(acac)_3$, S, OAm, TOP	HU	200, 260	578	56	22
AIGS	Ag(Ac), $In(Ac)_3$, TU, OAm, DDT, $Ga(acac)_3$	HU	150, 300	500−610	28	23
AIGSSe	Ag(Ac), $In(acac)_3$, $Ga(acac)_3$, TU, Se, OAm, DDT	HU	250	580−790	15−50	54
CGSe/ZnSe	CuI, $Ga(acac)_3$, Se, DDT, ODE, OAm, ZnI_2	HI	240	485−630	77.73	52
ACGSe	AgI, CuI, $Ga(acac)_3$, Se, OAm, DDT, ODE, ZnI_2	HI	240	510−620	71.9	24
AIGS/ZnS	AgI, $Ga(acac)_3$, S, OAm, DDT, $Zn(St)_2$	HI	305	460−671	2.5−32.3	51
AIS/ZnS	Ag(OAc), $In(OAc)_3$, $Zn(OAc)_2$, DDT, OAm, DMTU	HI	140, 150	643−745	28−59	59

[a]1-Octanethiol (OTT), 1-dodecanethiol (DDT), 1-octadecene (ODE), oleic acid (OA), oleylamine (OAm), *N*-hexylphosphonic acid (HPA), 1-tetradecylphosphonic acid (TDPA), octadecylphosphonic acid (ODPA), *N*,*N*′-dimethylthiourea (DMTU), tri-*n*-butyl phosphine (TBP), tri-*n*-octyl phosphine (TOP), trioctylamine (TOA), hexadecanethiol (HDT), hexadecylamine (HDA), diethyldithiocarbamate (DDTC), diphenylphosphine (DPP).

is easier to split into multiple sub-bands, which is the reason for the wider FWHM of CGS QDs than AGS ones. Simultaneously, Ga d-state would not split into substates under the action of surrounding crystal field like Cu d-state, making sure that the emission spectrum does not become wider. In conclusion, a proper design of direct band gap and adjustment of electronic band structure may be a promising direction for high-efficiency I−III−VI QDs and derivatives.

The ideal luminescence process usually consists of the following steps (instance for AgInGaS QDs in Figure 1b):[41] An electron is excited to CB by absorbing a high-energy photon, leaving a hole in the VB (step 1), and the excited electron relaxes to the band-edge to form an exciton with a hole. The exciton releases the photon by radiative recombination (step 2).

The donor−acceptor pair (DAP) recombination, as the main exciton recombination mode of I−III−VI QDs, should not be ignored (step 3). Most scientists support that the DAP emission of I−III−III QDs originate from their inherent defects, stemming from the recombination between excited electrons trapped by donor and holes trapped by acceptor respectively (step 3 in Figure 1b).[42] One of the salient features of DAP emission is the excitation power-dependent energy transfer, in which the peak energy of the PL spectrum shifts to the high-energy as the excitation power density increases. Similarly, temperature-dependent PL energy transfer related to DAP emission in AGS was reported by Marceddu et al., and the blue-shift of PL at 0−80 K is attributed to the increase in band gap caused by phonon interactions. Redjai et al. proved that the DAP spectrum as a function of donor−acceptor distance by measuring the binding energy of the acceptor (donor) in AIS monocrystal: As the distance between defects decreases, the coulomb-interaction energy increases. Furthermore, Tanaka et al. addressed that the integrated PL intensity of a S-poor sample was higher than that of stoichiometric sample, which suggests the S-defect related DAP emission may be one of the sources of PL.

Besides, thermodynamic quenching and nonradiative recombination always occurs under the effect of defects in crystal and surface, which manifests as defect trapping and Auger recombination (AR) (step 4). AR exacerbates energy loss, making the conductivity, optical properties, and radiation recombination rate worse.[10] In I−III−VI QDs, the defect (V_I, V_{III}, III_I and 2 V^-_I + III^{2+}_I) is the primary carrier of AR, the substitution of I and III cation disorder and lower defect formation energy increases the probability of defect formation.[16] Furthermore, the interaction between defect pairs may further reduce the defect formation energy. Hence, precisely regulate defects to suppress the AR and trap state is urgent strategy.

Bartłomiej et al. promoted two competitive recombination mechanisms to describe the influence of defects on recombing or quenching excitons in I−III−VI QDs, which is demonstrated in Figure 1c.[28] The two pathways for electron in the QDs are as follow: one is P1, the DAP emission mediated by the double charged trap state. Excitons get through the process of generating, being trapped, and radiatively recombining with the assistant of defects and the energy transferred to defect level reactivates, which is advantageous for improving the photoelectronic performance of high-defect-density I−III−VI QDs. Another is P2, the nonradiative (NR) process where carriers are competitively captured and blocked by NR centers, which mainly consist of surface-related defects, and coexist with intrinsic defects, leading to multiple paths of AR and trapping (the single NR-center and two NR-center). These models accurately describe the radiative recombination and nonradiative recombination approaches of I−III−VI QDs, and

https://doi.org/10.1021/acs.nanolett.2c03138
Nano Lett. XXXX, XXX, XXX−XXX

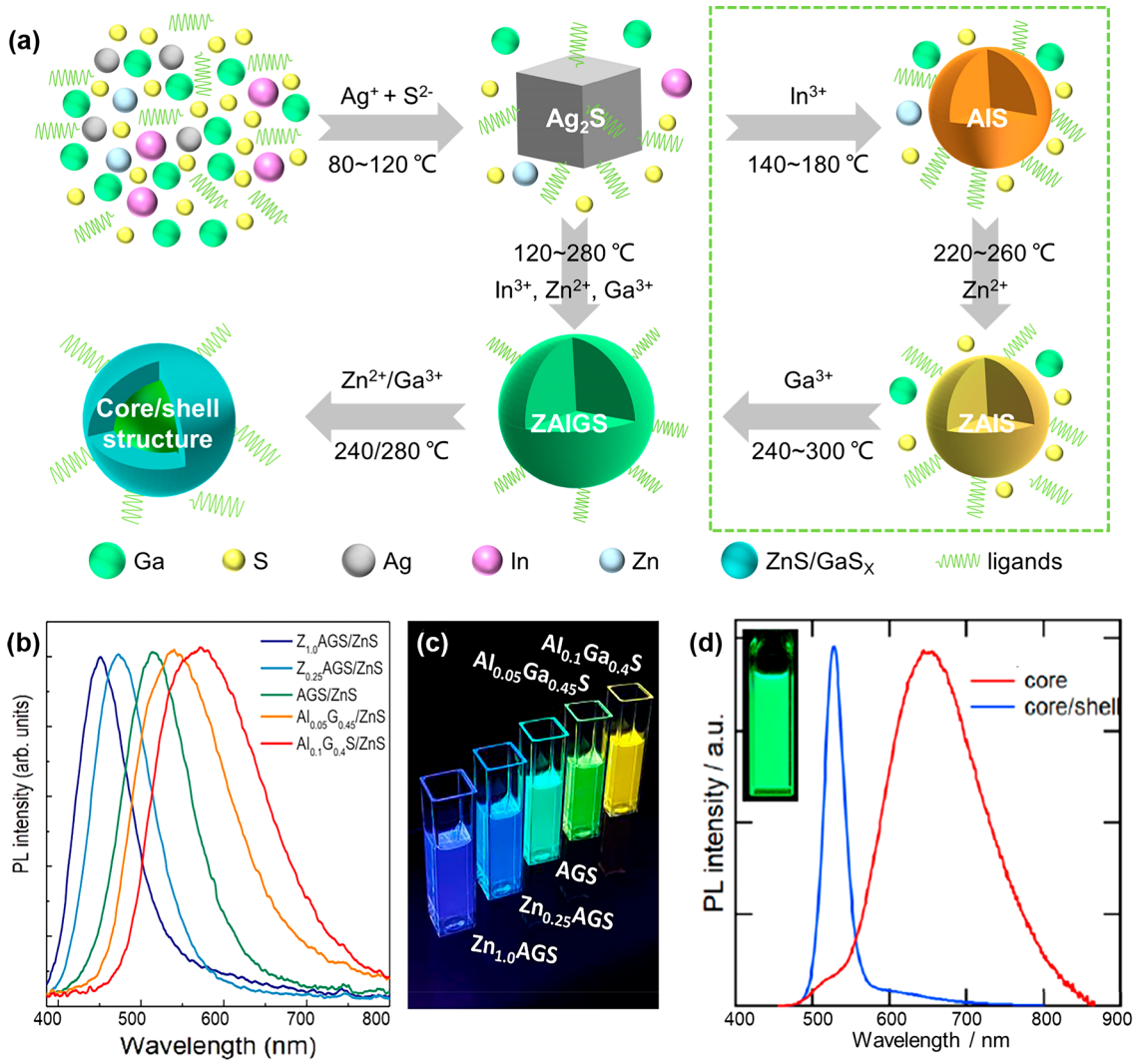

Figure 2. (a) General synthetic scheme of I−III−VI QDs and derivatives. (b) and (c) PL spectra and photograph of AIGS/ZnS QDs by adjusting the content of Zn^{2+}, Ga^{3+} and In^{3+}.[53] Adapted with permission from ref 53. Copyright 2018 Elsevier. (d) PL spectral comparison of $AgIn_xGa_{1-x}S_2$ (red) and $AgIn_xGa_{1-x}S_2/GaS_y$ (blue) QDs, the inset demonstrated picture of core/shell solution (E_x = 390 nm).[44] Adapted with permission from ref 44. Copyright 2023 American Chemical Society.

we provide a proposal for the synthesis of high-quality and low-defect QDs.

SYNTHESIS AND OPTICAL PROPERTIES

Because of the high formation energy of I−III−VI QDs and derivatives, the mainstream strategies of synthesizing QDs are still based on high temperature and organic phase medium, which produce QDs with good dispersion, excellent optical properties, high crystallinity, and high PLQY (~90%). The methods reported currently can be divided into hot-injection (HI), one-pot heating-up (HU), and single-source precursor thermal pyrolysis.[43−48] The HI method is the most adopted method for synthesizing quaternary/quinary QDs and especially shows great advantages in precisely constructing core/shell structure. The HU method may show superiority in the uniform nucleation and growth of QDs, and the reaction results can be controlled just by adjusting reaction temperature and precursor ratio. Single-source precursor thermal pyrolysis is almost the simplest synthesis scheme, while the ratio of ions and reaction process cannot be precisely regulated, which is the obstacle for preparation of high-efficiency and low-defect QDs. As for the aqueous-phase method, whose good biocompatibility is more suitable for the application of biological imaging (near-infrared). At the same time, the boiling point of water limits the preparation of QDs with good performance at high temperature (such as QDs with Ga^{3+}).[31]

Notably, the chemical activities among different ions (normally Ga^{3+}, Ag^{+}, Zn^{2+}, In^{3+}, S^{2-}) are unmatched, accompanied by the shortcomings of ternary QDs in adjusting composition, spectra, and efficiency; here the quaternary/quinary QDs and derivatives will be focused more on.

The synthesis of I−III−VI QDs and derivatives goes though the stages of nucleation, growth, and construction of the core/shell structure, which can be summarized as processes in Figure 3a. For the synthesis of ZAIS and ZAIGS QDs, Ag^{+} exhibits a high activity, tending to form Ag_2S cores (80−120 °C),[44] while the appropriate temperature for In^{3+}-doping is 140−180 °C to form $AgInS_2$ compounds.[49] Zn^{2+} and Ga^{3+} require higher temperatures of 220−260 °C (ZAIS) and 240−300 °C (ZAIGS) to efficiently enter the lattice, respectively. The temperature steps effectively avoid defects in the inhomogeneous nucleation process.

https://doi.org/10.1021/acs.nanolett.2c03138
Nano Lett. XXXX, XXX, XXX−XXX

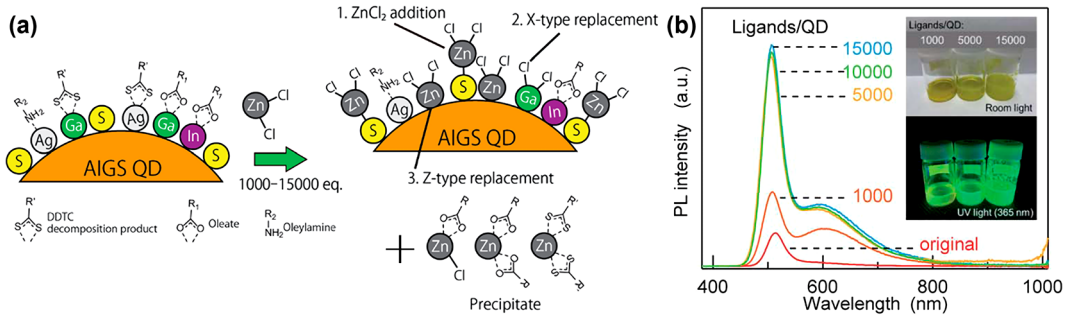

Figure 3. (a) Schematic diagram of ligands passivating AIGS/GaS_y QDs. (b) PL spectra and photographs of QDs after ligand passivation with $ZnCl_2$.[20] Adapted with permission from ref 20. Copyright 2022 Royal Society of Chemistry, under CC BY 3.0.

Actually, the specific experimental conditions, such as ionic chemical activity, temperature, ligand, and core/shell structure, are considered to be the key factors inspiring the improvement strategies of I−III−VI QDs and derivatives. The experimental conditions and optical properties are summarized in Table 1.

Control of Reaction Conditions. The key to the successful preparation of spectral adjustable and efficient QDs is to regulate the chemical activity of different ions and inhibit crystal/surface defects, where the synthesis temperature and selection/dosage of precursors play crucial roles. The compositional dependence enables the PL and PLQY of $CI_{0.5}G_{0.5}S$ and $CI_{0.3}G_{0.7}S$ to be regulated as 479−500 nm and 20−85%, respectively.[50] Similarly, varying the content of Ga^{3+}, In^{3+}, Ag^+, or S^{2-} can adjust the wavelength from 630 to 485 nm and further expand the coverage of emission toward shorter wavelength by Zn^{2+}-doping.[51,52] Yang et al. achieved a blue I−III−VI derivative QDs by regulating the doping amount of Zn^{2+} ($Z_{1.0}$AGS/ZnS), thus making the PL blue-shifted to 450 nm, accompanied by a PLQY of 64% (Figure 2b,c).[53] Besides, due to different chemical activity at a same temperature, the PL of AIGS QDs is nonlinearly consistent with the feed ratio of In^{3+}/Ga^{3+}, leading to an uneven element distribution.[54,55] It worth noting that Ga^{3+} can effectively passivate the shallow defect energy level and weaken the DAP process, which may be the origination of narrow FWHM of Ga^{3+} doped ZAIGS QDs.[27] Although Ga^{3+} has low chemical activity and a relatively slow incorporation rate into the lattice, the selection of suitable Ga^{3+} and S^{2-} source (e.g., $Ga(DDTC)_3$ and DMTU) and higher temperature can be a proper solution.[47,56] Simultaneously, Zn^{2+}-doping is reported as an efficient strategy in reducing the concentration of cation vacancy (V_{In}, V_{Ga}), which can in turn eliminate nonradiative recombination center and improve PLQY. The CGS QDs get a high PLQY of 77.73% passivated by $Zn(St)_2$, whose lower reactivity is more favorable to passivate the surface defects.[52] Furthermore, the V_{defect} level is closely related to Ag^+, where less V_{Ag} endows QDs strong radiative recombination process by enhancing DAP emission, thus improving PLQY to 58−69%.[53]

Core/Shell Structure. The construction of quantum-well core/shell structure is an effective way to passivate the defects, improve the PLQY, convergence energy and narrow the FWHM of QDs. The existed difficulty of constructing core/shell structure is the low-defect passivation efficiency, which hinges on the poor lattice matching and inferior charge injection resulting from the thick shell.

ZnS is the most reported shell in I−III−VI QDs,[53] its wide direct band gap limits the energy scattering of core, and the surface binding passivates the defects of QDs.[59] Yu et al. synthesized an $AgIn_5S_8$/ZnS core−shell structure QDs by successively injecting S-precursor and Zn-precursor, benefited by lower surficial defect density, the QDs demonstrated potential in high-efficiency LEDs.[60] Furthermore, multiple cladding successfully achieves an increased passivation effect.[61] Interestingly, excessive alloying process of Zn^{2+} would break down the crystal structure of I−III−VI QDs, and seriously hinder the subsequent shell forming process,[25] which may be the fundamental obstacle for obtaining high-quality QDs with a large amount of Zn^{2+}-precursor.

However, the unfavorable lattice matching between core and shells caused by thicker and uncontrollable ZnS may adversely affect the luminescent properties, such as intermediate energy level and higher turn-on voltage in optoelectronic devices,[10] which means that the effect of ZnS shell in narrowing the spectra of QDs is unobvious. GaS_x shell is considered as an idea candidate for synthesizing narrow-FWHM core/shell QDs.[21,22,57] Kuwabata et al. realized a narrow-FWHM (31 nm) $AgIn_xGa_{1-x}S_2/GaS_y$ QDs by passivating defects with GaS_y (Figure 2d).[44] Usually, the GaS_x shell exists as an amorphous phase, which is more conducive to the stability of various lattice plane and defects,[22] even though there still remains the "shoulder peak", which is probably caused by hybrid phase and incomplete passivation of defect-related emission. Correspondingly, In_2S_3 is also reported as shell material in AIS QDs to enhance the band-edge emission,[49] nevertheless, a more pronounced tail in spectra always can be discovered, which may originate from the emission of small $AgIn_5S_8$ byproducts.

Ligand Engineering. Ligand is a crucial factor for precise regulating the photoelectric properties of QDs, and exerts influence on the synthesis and post-treatment process of QDs. However, there only few ligands have been reported for enhancing the performance of I−III−VI QDs and derivatives. The effect of ligands on QDs can be concluded as the following aspects: (i) Adjusting energy level. Li et al. found that the use of phosphoric acid ligands with different dipoles can change the energy level of AIGS QDs, as phosphoric acid with long alkyl chain can move both CBM and VBM toward higher energy.[5] (ii) Regulating the phase and size of QDs. Long alkane chain thiols and primary alkylamines can contribute to the formation of orthonormal AGS phase, whereas employing a TOA yields a mixture of tetragonal AGS and Ag_9GaS_6.[62] Furthermore, increasing the proportion of OA makes the size of prepared-QDs significantly smaller, and OA is effective in passivating QDs more strongly than OAm, thus preventing the unnecessary byproducts. In contrast, excessive OAm can reduce the nucleation sites, and thus promote the growth of QDs to form the larger QDs.[62] (iii) Defects

https://doi.org/10.1021/acs.nanolett.2c03138
Nano Lett. XXXX, XXX, XXX−XXX

Table 2. Performance Summary of E-/B-WLEDs of I−III−VI QDs and Derivatives[a]

QDs	CRI	CCT [K]	V_{on} [V]	L_{max} [cd m^{-2}]	EQE [%]	E_x [nm]	ref.
CGS	83−88	7494−8234	∼5	1007	1.9		35
CGS, CIS	82	3995−6046	∼4	2172	4.6		10
CGS	87−90	3796−4447	∼5	2135	3.8		6
CGS	82−84	5527−5919				400	63
CGS:Mn/ZnS	83−87	3651−5410				400	58
CGS:Mn/ZnS	65−95	6417−7884				450	64
ACGSe		3221−15170				450	24
AIGS	90.33	5947				450	55
	89.07	2451				400	

[a]Color rendering index (CRI), correlated color temperature (CCT).

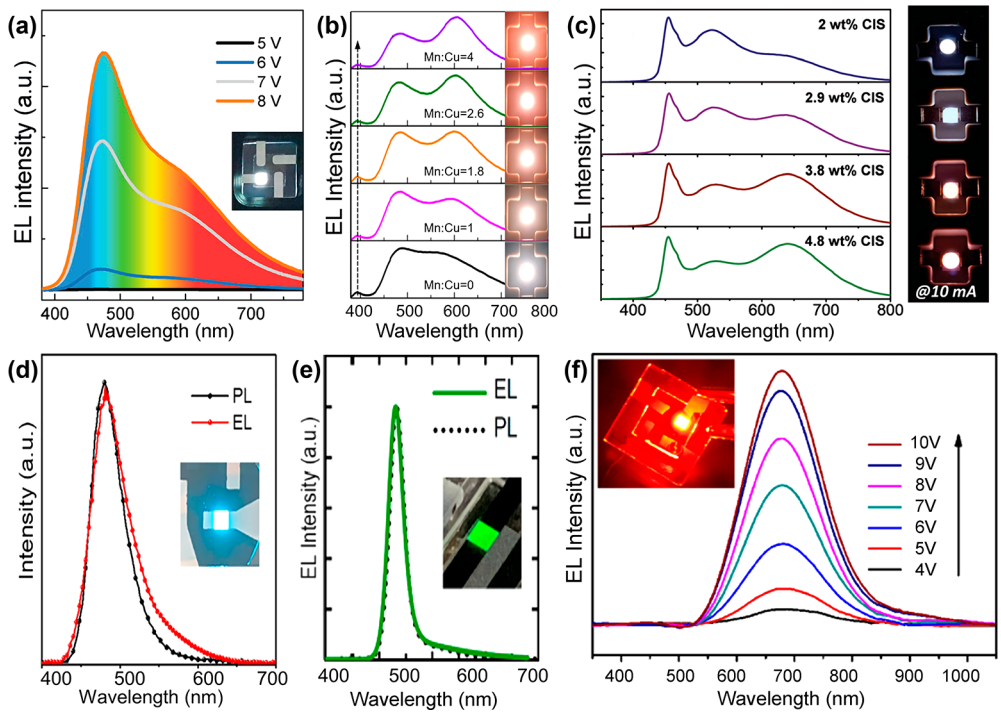

Figure 4. (a) EL spectra under voltage of single-QD based WLED, the inset demonstrated the device in action.[35] Adapted with permission from ref 35. Copyright 2016 WILEY-VCH. (b) Spectra of CGS:Mn/ZnS WLEDs with different Mn-content.[58] Adapted with permission from ref58. Copyright 2016 American Chemical Society. (c) Spectra of down-converter WLEDs, whose emitter consists of a mixture of CGS and CIS QDs.[65] Adapted with permission from ref 65. Copyright 2017 Royal Society of Chemistry. (d)−(f) EL spectra of blue, green, and red QDs, and the photographs demonstrate the LEDs under voltages.[26,34,45] Adapted with permission from ref 26 (copyright 2022 American Chemical Society), ref 34 (copyright 2018 The Optical Society of American, under CC BY 4.0), and ref 45 (copyright 2023 American Chemical Society).

passivation. The Z-type ligands including Lewis-acidic metal complexes, can coordinated with unsaturated electron defects (V_S and V_{Se}), the schematic diagram of ligand passivation is shown in Figure 3a.[20] Kuwabata et al. reported that Z-type ligand like MX_n ($ZnCl_2$, $Zn(Ac)_2$, $InCl_3$, $GaCl_3$) not only binds to the dangling sulfur defect but also provides the X^- that eventually removes the original ligands through ligand exchange, so the AIGS QDs treated by $ZnCl_2$ can get a high PQLY of 73.4% (Figure 3b).[20] Moreover, $Ga(DDTC)_3$ can be bound to AIGS core as Z-type ligands, which will react smoothly to release Ga^{3+} and S^{2-} on the surface of core to build a core/shell structure. Ligands such as TOP, TBP, and DDP are also reported to increase the PLQY (up to 56%−68%) of I−III−VI QDs and derivatives.[6,22,56]

LED APPLICATIONS

As mentioned above, I−III−VI QDs and derivatives demonstrate large Stokes shifts and broader FWHM, which have excellent performance in downconverters electronic and backlight white LEDs (E-/B-WLEDs), the performance of WLEDs are given in Table 2.

Usually, single-QDs emitters are the best choice for E-WLEDs for bias-insensitive color stability and high efficiency, the main limitation is the difficulties in regulating the location of radiative recombination centers and broadening the emission spectra. Reasonably designing various recombination channels in QDs to achieve energy transfer is a feasible strategy for high-CRI WLEDs. Yang et al. obtained all-solution processed single-QDs E-WLEDs and flexible planar device by regulating the ratio of Cu^+/Ga^{3+} (Figure 4a),[35] whose DAP recombination enhanced the emission near 600 nm (originating from CB-V_{Cu} transition). The EL spectra indicative of

https://doi.org/10.1021/acs.nanolett.2c03138
Nano Lett. XXXX, XXX, XXX−XXX

Table 3. Performance Summary of RGB-QLEDs Based on I−III−VI QDs and Derivatives[a]

QDs	EL [nm]	FWHM [nm]	V_{on} [V]	L_{max} [cd m^{-2}]	CE [cd A^{-1}]	EQE [%]	ref.
ZAGS	470	48	3.2	123.1	0.62	0.4	26
CGS	475	∼75	∼4	1404	11.8	7.1	10
CGS	∼479	∼175	∼5.8	∼39	0.01	0.007	50
$CI_{0.3}G_{0.7}S$	∼538	∼125	∼5.5	∼300	0.05	0.023	
$CI_{0.5}G_{0.5}S$	∼558	∼130	∼4.8	∼900	1.65	0.6	
CGS	495	∼80	∼4.4	1474		2.5	9
AGS	500	∼200	∼5.1	124		0.2	
AIGS	570	44	2.8	60.3		0.54	11
AIGS/GaS_x	531	33	2.4	175		1.1	45
CGS	472	∼75	∼5	643	8.2	5.1	6
CGSSe	540	∼100	∼5.5	3921	17.8	5.2	
CGSe	629	∼110	∼5.5	2021	5.1	4.7	
CIS/ZnS	602	∼110	∼3	8464	18.2	7.3	66
CIS/ZnS	620	∼75	∼2.8	113.83	0.48	3.36	34

[a]Luminance (L), current efficiency (CE).

radiative recombination of injected carriers were well confined to CGS/ZnS emitting layer. Notably, the DAP emission gets worse with voltage increase, which seriously hinders the color stability of single-QDs E-WLEDs.

I−III−VI QDs and derivatives demonstrate a negligible reactivity among various QDs, which is conductive to construct single-layer mixed-QDs emitting layer. In 2019, Yang et al. fabricated E-WLEDs by mixing ZCGS (blue) and CIS (yellow) in different proportions, and finally got a high-efficiency E-WLEDs (EQE = 4.6%) with CRI of 81−82.[10] Interestingly, the FRET between ZCGS and CIS QDs contributes the balanced emission.

B-WLEDs are easier to achieve than E-WLEDs, since the carrier injection and transport of the former can be ignored. The UV/blue LEDs chip is needed as the backlight to excite QDs, and its brightness and performance are closely related to the luminous power of the chip, composition, PLQY of QDs and thermodynamic quenching of excitons.

The energy transfer of Mn^{2+} is considered as an ideal choice for compensating the deficient DAP emission and expanding the emission range, which provides an alternative for B-WLEDs. As shown in Figure 4b, a systematic white spectra evolution can be achieved by regulating the Mn^{2+} concentration.[58,64] As mentioned before, the insignificant reactivity of QDs makes it viable for construction of mixed-QDs B-WLEDs with near-ideal CRI and CCT (Figure 4c), in which the proportion CIS QDs contribute the red-range emission.[65]

As for monochrome display (RGB-QLEDs), I−III−VI QDs and derivatives lag behind, primarily resulting from their low color purity. Meanwhile, the deficiencies of synthesis method and the complex luminescence mode also leads to the low efficiency of LEDs. The main specifications and development tendency are summarized in Table 3.

Yang et al. constructed early QLEDs in the blue, green, and yellow regions, respectively.[50] However, insufficient regulating and passivating strategies leads to shortcomings: "green" QLED generally emits yellow light because of greater FWHM (>120 nm), and "blue" QLED is accompanied by multiple EL peaks. The characteristics of QLEDs are strongly dependent on the composition, showing decreases in efficiency with increasing Ga^{3+} content. In 2018, Yang et al. integrated QLEDs based on AGS and CGS QDs to discuss the effect of composition and electronic structure on efficiency.[9] The results indicate that the EL of AGS is broadened compared with the PL, while that of CGS is nearly equivalent to PL. The main reason may be related to the excitonic coupling to longitudinal optical photons under electric field. More surface-defect AGS are likely to provoke a higher degree of phonon coupling. Even so, Ag−Ga-based QDs are still the best candidate for preparing blue LEDs. Tang et al. reported the narrowest blue QLEDs (48 nm) based on Ag−Ga−Zn−S QDs (Figure 4d), the ratios of cations (Ag^+/Zn^{2+} and Ag^+/Ga^{3+}) are the crucial for narrow emission.[26] This research provides a feasible strategy for pure-monochrome emission. Tsuzuki et al. reported a GaS_x-passivated AIGS QD, whose defect sites are compensated, and the defect-related direct electron injection are suppressed. As shown in Figure 4e, the fabricated QLED demonstrated a narrowest green electronic emission (33 nm).[45] For red LEDs, a common strategy is fabricating with CIS/ZnS QDs as luminous layer, whose strong DAP emission and high PLQY are beneficial to LEDs with low turn-on voltage (2.8 V) and high EQE (3.36%) (Figure 4f).[34] However, the researches in narrowing the FWHM of R-QLEDs are still backward (usually larger than 100 nm), and efficiency improvements of RGB-QLEDs also need to be further developed.

One of the inevitable problems for monochromatic QDs is the spectral stability under voltage. The FRET and Auger excited state become more sensitive to lower bang gap, resulting in an crescendo red emission as the voltage increases, which can be prevented by thicker shells and effective surface passivation.[10] Interestingly, the energy level of defects are close-proximity to the band edge in red QDs, hence red LEDs exhibit better electrogenic spectral stability than other monochromatic LEDs.

OUTLOOK

In summary, I−III−VI QDs and derivatives were introduced in detail from the perspectives of electronic energy structure, luminescence mechanism, synthesis, optical properties, and LEDs, which are expected to be excellent candidates for traditional II−VI, III−V, and perovskite QDs.

For the current I−III−VI QDs and derivatives, the necessary strategies and directions should be proposed to better promote the development of high-efficiency and stable QDs,[67−70] especially in synthetic strategy improvement and post treatment. For the applications of LEDs, the I−III−VI QDs and derivatives demonstrate promising prospect in WLEDs

https://doi.org/10.1021/acs.nanolett.2c03138
Nano Lett. XXXX, XXX, XXX−XXX

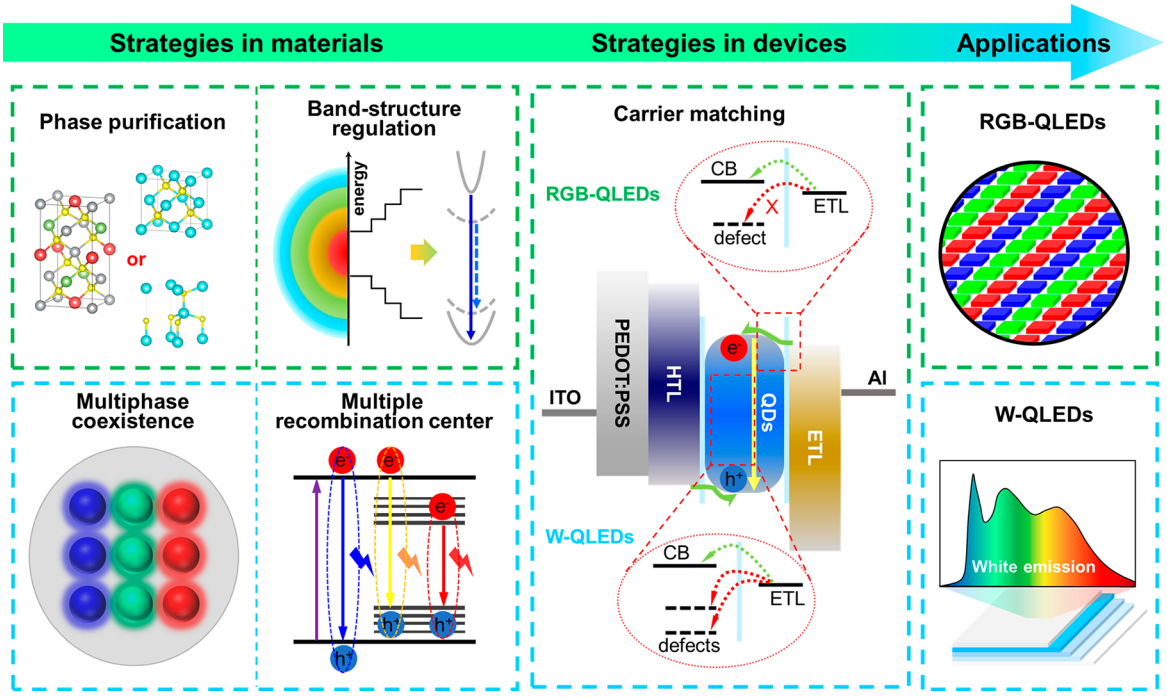

Figure 5. Schematic diagram summarizes the strategies, solutions, and the application prospects of I−III−VI QDs and derivatives in monochrome and white-QLEDs.

benefiting from their broader FWHM and complex emissive mechanism. Comparatively, although the progress of RGB-LEDs lags behind, there is still the prospect of further optimization. According to DFT calculation, it is possible to achieve high luminous efficiency and color purity. Specifically, the improvement strategy of QDs and devices can be concluded in Figure 5.

Strategies in RGB-QDs. Monochrome displays require strict demands on the crystal structure and energy band.

(i) Phase purification. Thermodynamically regulating the transition of different crystal phases can provide ideas for the pure phase preparation of I−III−VI QDs and derivatives.[70] Furthermore, pure/ordered (hetero) phase can be realized by investigating phase purification and high-efficiency hetero-structure construction process, such as ion activity regulation, phase diagram, gradient temperature control, and ligand passivation.

(ii) Band structure regulation. First, the first-principles calculation of the excited-state dynamic behavior about I−III−VI QDs and derivatives may be an instructive design to quantitatively describe physical characteristics such as band-edge dispersion, density of states, and transition dipole moment.[71] Second, construction of efficient pure/ordered phase and heterostructure are effective strategies to converge excited state energy. Based on the composition-dependent energy band, energy transmission channels can be built through ion doping and type-I core/shell heterostructure to reduce the energy loss of excited states. The special surface anion-rich quantum well structure may be another effective shell to converge the energy.[67]

Strategies in White-Emission QDs. Different from the energy-convergence design of monochromatic QDs, the white-emission QDs refer multiple recombination centers and broader emissive range.

(i) Multiphase coexistence. The different emission spectra of various phases should be considered as an advantage for fabricating white emission with desired CRI, which can be obtained by adjusting the ratio of phases.

(ii) Multiple recombination centers. Fully exploring the favorable factors of defect energy levels in the regulation of energy band structure of QDs, and accurately designing the radiative recombination centers, can provide guidance for excitons to transfer among multiple energy levels, which is beneficial for the broad and multicenter emission. Drawing on the methodology of ZnO QDs, whose luminescence mechanism is controlled by defects, may guide further exploration of the internal energy transfer and regulation method in I−III−VI QDs and derivatives.[68]

Strategies for QLEDs. Combining the application requirements of RGB- and W-QLEDs with low-cost conductive polymers, deep-level HTL, interface passivation layers to match the energy level of QDs are the major concerns on the device, which are the foundations of efficient carrier injection-transport-combination system.

(i) The surface ligands and shell thickness of QDs are the primary obstacles for carrier injection. Appropriate polarity purification reagent can effectively accommodate the surface state of QDs and enhance carrier injection.[72]

(ii) In terms of QLEDs, both bilateral surface passivation and the construction of gradient electron transport layer can effectively enhance the balance of carrier injection and transport, thus improving device efficiency.[73]

(iii) Correspondingly, carrier recombination mechanism and region regulation are also effective strategies for QLEDs, and novel device structures with low FRET and Auger quenching also need to be developed.

There is no doubt that lots of researches should be done to achieve a breakthrough, and I−III−VI QDs and derivatives, as environmentally friendly QDs with designable radiative recombination center, indicate superior potential in the development of high-efficiency monochrome and white-emitting applications.

https://doi.org/10.1021/acs.nanolett.2c03138
Nano Lett. XXXX, XXX, XXX−XXX

AUTHOR INFORMATION

Corresponding Authors

Shuai Zhang − *MIIT Key Laboratory of Advanced Display Materials and Devices, Institute of Optoelectronics & Nanomaterials, School of Materials Science and Engineering, Nanjing University of Science and Technology, Nanjing 210094, China*; Email: zs0601@njust.edu.cn

Heesun Yang − *Department of Materials Science and Engineering, Hongik University, Seoul 121-791, Korea*; orcid.org/0000-0002-2827-2070; Email: hyang@hongik.ac.kr

Haibo Zeng − *MIIT Key Laboratory of Advanced Display Materials and Devices, Institute of Optoelectronics & Nanomaterials, School of Materials Science and Engineering, Nanjing University of Science and Technology, Nanjing 210094, China*; orcid.org/0000-0002-0281-3617; Email: zeng.haibo@njust.edu.cn

Authors

Linxiang Yang − *MIIT Key Laboratory of Advanced Display Materials and Devices, Institute of Optoelectronics & Nanomaterials, School of Materials Science and Engineering, Nanjing University of Science and Technology, Nanjing 210094, China*

Bo Xu − *MIIT Key Laboratory of Advanced Display Materials and Devices, Institute of Optoelectronics & Nanomaterials, School of Materials Science and Engineering, Nanjing University of Science and Technology, Nanjing 210094, China*; orcid.org/0000-0002-4703-7340

Jiangyuan Jiang − *MIIT Key Laboratory of Advanced Display Materials and Devices, Institute of Optoelectronics & Nanomaterials, School of Materials Science and Engineering, Nanjing University of Science and Technology, Nanjing 210094, China*

Bo Cai − *State Key Laboratory for Organic Electronics and Information Displays & Institute of Advanced Materials (IAM), Nanjing University of Posts & Telecommunications (NUPT), Nanjing 210023, China*

Xinyi Lv − *MIIT Key Laboratory of Advanced Display Materials and Devices, Institute of Optoelectronics & Nanomaterials, School of Materials Science and Engineering, Nanjing University of Science and Technology, Nanjing 210094, China*

Yousheng Zou − *MIIT Key Laboratory of Advanced Display Materials and Devices, Institute of Optoelectronics & Nanomaterials, School of Materials Science and Engineering, Nanjing University of Science and Technology, Nanjing 210094, China*; orcid.org/0000-0001-5834-5579

Zhiyong Fan − *Department of Electronic & Computer Engineering, The Hong Kong University of Science and Technology, Kowloon, Hong Kong China*; orcid.org/0000-0002-5397-0129

Complete contact information is available at: https://pubs.acs.org/10.1021/acs.nanolett.2c03138

Author Contributions

[⊥]L.Y. and S.Z. contributed equally to this work. L.Y. and S.Z.: conceptualization, software, writing. L.Y., S.Z., J.J., B.C., and X.L.: investigation, drawing. S.Z., B.X., Y.Z., Z.F., H.Y., and H.Z.: supervision, writing - review and editing.

Notes

The authors declare no competing financial interest.

ACKNOWLEDGMENTS

This work was supported by the National Natural Science Foundation of China (Nos. 52131304 and 22279059), Jiangsu Funding Program for Excellent Postdoctoral Talent (2022ZB249), the China Postdoctoral Science Foundation (2022M721621), Cooperative R&D of photoelectric energy integrated devices (BZ2020063), the National Research Foundation of Korea (NRF) grant (2015R1A6A1A03031833), and Fundamental Research Funds for the Central Universities (No. 30921011106).

REFERENCES

(1) Deng, Y.; Peng, F.; Lu, Y.; Zhu, X.; Jin, W.; Qiu, J.; Dong, J.; Hao, Y.; Di, D.; Gao, Y.; et al. Solution-processed green and blue quantum-dot light-emitting diodes with eliminated charge leakage. *Nat. Photonics* **2022**, *16*, 505−511.

(2) Liu, X.-K.; Xu, W.; Bai, S.; Jin, Y.; Wang, J.; Friend, R. H.; Gao, F. Metal halide perovskites for light-emitting diodes. *Nat. Mater.* **2021**, *20* (1), 10−21.

(3) Song, J.; Li, J.; Li, X.; Xu, L.; Dong, Y.; Zeng, H. Quantum Dot Light-Emitting Diodes Based on Inorganic Perovskite Cesium Lead Halides ($CsPbX_3$). *Adv. Mater.* **2015**, *27* (44), 7162−7167.

(4) Li, H.; Zhang, W.; Bian, Y.; Ahn, T. K.; Shen, H.; Ji, B. ZnF_2-Assisted Synthesis of Highly Luminescent InP/ZnSe/ZnS Quantum Dots for Efficient and Stable Electroluminescence. *Nano Lett.* **2022**, *22* (10), 4067−4073.

(5) Li, F.; Wei, J.; Liao, G.; Guo, C.; Huang, Y.; Zhang, Q.; Jin, X.; Jiang, S.; Tang, Q.; Li, Q. Quaternary quantum dots with gradient valence band for all-inorganic perovskite solar cells. *J. Colloid Interface Sci.* **2019**, *549*, 33−41.

(6) Yoon, S.-Y.; Kim, Y.-H.; Jo, D.-Y.; Jo, J.-H.; Lee, S.-H.; Kim, H.-M.; Kim, Y.; Kim, S.-K.; Yang, H. Efficient synthesis of multinary Zn-Cu-Ga-$Se_{1-x}S_x$ quantum dots as full visible-covering emitters and their tricolored white electroluminescence. *Chem. Eng. J.* **2021**, *410*, 128426−128435.

(7) Septina, W.; Sugimoto, M.; Chao, D.; Shen, Q.; Nakatsuka, S.; Nose, Y.; Harada, T.; Ikeda, S. Photoelectrochemical water reduction over wide gap (Ag,Cu)(In,Ga)S_2 thin film photocathodes. *Phys. Chem. Chem. Phys.* **2017**, *19* (19), 12502−12508.

(8) Kameyama, T.; Yamauchi, H.; Yamamoto, T.; Mizumaki, T.; Yukawa, H.; Yamamoto, M.; Ikeda, S.; Uematsu, T.; Baba, Y.; Kuwabata, S.; Torimoto, T. Tailored Photoluminescence Properties of Ag(In,Ga)Se_2 Quantum Dots for Near-Infrared In Vivo Imaging. *ACS Appl. Nano Mater.* **2020**, *3* (4), 3275−3287.

(9) Kim, J. H.; Yoon, S. Y.; Kim, K. H.; Lim, H. B.; Kim, H. J.; Yang, H. Electroluminescence from two I-III-VI quantum dots of A-Ga-S (A = Cu, Ag). *Opt. Lett.* **2018**, *43* (21), 5287−5290.

(10) Yoon, S.-Y.; Kim, J.-H.; Kim, K.-H.; Han, C.-Y.; Jo, J.-H.; Jo, D.-Y.; Hong, S.; Hwang, J. Y.; Do, Y. R.; Yang, H. High-efficiency blue and white electroluminescent devices based on non-Cd I−III−VI quantum dots. *Nano Energy* **2019**, *63*, 103869−103875.

(11) Motomura, G.; Ogura, K.; Iwasaki, Y.; Uematsu, T.; Kuwabata, S.; Kameyama, T.; Torimoto, T.; Tsuzuki, T. Electroluminescence from band-edge-emitting $AgInS_2/GaS_x$ core/shell quantum dots. *Appl. Phys. Lett.* **2020**, *117* (9), 091101−091106.

(12) Chen, B.; Pradhan, N.; Zhong, H. From Large-Scale Synthesis to Lighting Device Applications of Ternary I-III-VI Semiconductor Nanocrystals: Inspiring Greener Material Emitters. *J. Phys. Chem. Lett.* **2018**, *9* (2), 435−445.

(13) Kim, T.; Kim, K. H.; Kim, S.; Choi, S. M.; Jang, H.; Seo, H. K.; Lee, H.; Chung, D. Y.; Jang, E. Efficient and stable blue quantum dot light-emitting diode. *Nature.* **2020**, *586* (7829), 385−389.

(14) Olejniczak, A.; Cichy, B.; Stręk, W. DFT calculations of metal-organic I-III-VI semiconductor clusters: Benchmark of exchange-correlation functionals and localized basis sets. *Comput. Mater. Sci.* **2019**, *163*, 186−195.

https://doi.org/10.1021/acs.nanolett.2c03138
Nano Lett. XXXX, XXX, XXX−XXX

(15) Leach, A. D.; Macdonald, J. E. Optoelectronic Properties of $CuInS_2$ Nanocrystals and Their Origin. *J. Phys. Chem. Lett.* **2016**, *7* (3), 572−583.
(16) Coughlan, C.; Ibanez, M.; Dobrozhan, O.; Singh, A.; Cabot, A.; Ryan, K. M. Compound Copper Chalcogenide Nanocrystals. *Chem. Rev.* **2017**, *117* (9), 5865−6109.
(17) Baimuratov, A. S.; Martynenko, I. V.; Baranov, A. V.; Fedorov, A. V.; Rukhlenko, I. D.; Kruchinin, S. Y. Giant Stokes Shifts in $AgInS_2$ Nanocrystals with Trapped Charge Carriers. *J. Phys. Chem. C* **2019**, *123* (26), 16430−16438.
(18) Liu, Z.; Liu, J.; Huang, Y.; Li, J.; Yuan, Y.; Ye, H.; Zhu, D.; Wang, Z.; Tang, A. From one-dimensional to two-dimensional wurtzite $CuGaS_2$ nanocrystals: non-injection synthesis and photocatalytic evolution. *Nanoscale* **2019**, *11* (1), 158−169.
(19) Bhattacharyya, B.; Pandey, A. $CuFeS_2$ Quantum Dots and Highly Luminescent $CuFeS_2$ Based Core/Shell Structures: Synthesis, Tunability, and Photophysics. *J. Am. Chem. Soc.* **2016**, *138* (32), 10207−10213.
(20) Hoisang, W.; Uematsu, T.; Torimoto, T.; Kuwabata, S. Surface ligand chemistry on quaternary $Ag(In_xGa_{1-x})S_2$ semiconductor quantum dots for improving photoluminescence properties. *Nanoscale Adv.* **2022**, *4* (3), 849−857.
(21) Hoisang, W.; Uematsu, T.; Yamamoto, T.; Torimoto, T.; Kuwabata, S. Core Nanoparticle Engineering for Narrower and More Intense Band-Edge Emission from $AgInS_2/GaS_x$ Core/Shell Quantum Dots. *Nanomaterials* **2019**, *9* (12), 1763−1778.
(22) Uematsu, T.; Wajima, K.; Sharma, D. K.; Hirata, S.; Yamamoto, T.; Kameyama, T.; Vacha, M.; Torimoto, T.; Kuwabata, S. Narrow band-edge photoluminescence from $AgInS_2$ semiconductor nanoparticles by the formation of amorphous III−VI semiconductor shells. *NPG Asia Mater.* **2018**, *10* (8), 713−726.
(23) Kameyama, T.; Kishi, M.; Miyamae, C.; Sharma, D. K.; Hirata, S.; Yamamoto, T.; Uematsu, T.; Vacha, M.; Kuwabata, S.; Torimoto, T. Wavelength-Tunable Band-Edge Photoluminescence of Non-stoichiometric Ag-In-S Nanoparticles via Ga^{3+} Doping. *ACS Appl. Mater. Interfaces* **2018**, *10* (49), 42844−42855.
(24) Wei, J.; Hu, Z.; Zhou, W.; Qiu, Y.; Dai, H.; Chen, Y.; Cui, Z.; Liu, S.; He, H.; Zhang, W.; Xie, F.; Guo, R. Emission tuning of highly efficient quaternary Ag-Cu-Ga-Se/ZnSe quantum dots for white light-emitting diodes. *J. Colloid Interface Sci.* **2021**, *602*, 307−315.
(25) Kim, B. Y.; Kim, J. H.; Lee, K. H.; Jang, E. P.; Han, C. Y.; Jo, J. H.; Jang, H. S.; Yang, H. Synthesis of highly efficient azure-to-blueemitting Zn-Cu-Ga-S quantum dotsSynthesis of highly efficient azure-to-blue-emitting Zn-Cu-Ga-S quantum dots. *Chem. Commun.* **2017**, *53* (29), 4088−4091.
(26) Xie, X.; Zhao, J.; Lin, O.; Yin, Z.; Li, X.; Zhang, Y.; Tang, A. Narrow-Bandwidth Blue-Emitting Ag-Ga-Zn-S Semiconductor Nanocrystals for Quantum-Dot Light-Emitting Diodes. *J. Phys. Chem. Lett.* **2022**, *13* (51), 11857−11863.
(27) Galiyeva, P.; Rinnert, H.; Balan, L.; Alem, H.; Medjahdi, G.; Uralbekov, B.; Schneider, R. Single-source precursor synthesis of quinary AgInGaZnS QDs with tunable photoluminescence emission. *Appl. Surf. Sci.* **2021**, *562*, 150143−150150.
(28) Olejniczak, A.; Rich, R.; Gryczynski, Z.; Cichy, B. Non-excitonic defect-assisted radiative transitions are responsible for new D-type blinking in ternary quantum dots. *Nanoscale Horizons* **2021**, *7* (1), 63−76.
(29) Morselli, G.; Villa, M.; Fermi, A.; Critchley, K.; Ceroni, P. Luminescent copper indium sulfide (CIS) quantum dots for bioimaging applications. *Nanoscale Horizons* **2021**, *6* (9), 676−695.
(30) Bai, X.; Purcell-Milton, F.; Gun'ko, Y. K. Near-infrared-emitting CIZSe/CIZS/ZnS colloidal heteronanonail structures. *Nanoscale* **2020**, *12* (28), 15295−15303.
(31) Silva, R. R.; Freitas, D. V.; Sousa, F. L. N.; Jesus, A. C.; Silva, S. E.; Mansur, A. A. P.; Carvalho, S. M.; Marques, D. S.; Carvalho, I. C.; Azevedo, W. M.; Mansur, H. S.; Navarro, M. Synthesis of $CuInS_2$ and $CuInS_2$@ZnX (X = S, Se) nanoparticles for bioimaging of cancer cells using electrochemically generated S^{2-} and Se^{2-}. *J. Alloys Compd.* **2021**, *853*, 156926−156938.
(32) Hinterding, S. O. M.; Berends, A. C.; Kurttepeli, M.; Moret, M.-E.; Meeldijk, J. D.; Bals, S.; van der Stam, W.; de Mello Donega, C. Tailoring Cu^+ for Ga^{3+} Cation Exchange in $Cu_{2-x}S$ and $CuInS_2$ Nanocrystals by Controlling the Ga Precursor Chemistry. *ACS Nano* **2019**, *13* (11), 12880−12893.
(33) Hansen, E. C.; Liu, Y.; Utzat, H.; Bertram, S. N.; Grossman, J. C.; Bawendi, M. G. Blue Light Emitting Defective Nanocrystals Composed of Earth-Abundant Elements. *Angew. Chem., Int. Ed.* **2020**, *59* (2), 860−867.
(34) Li, F.; Guo, C.; Pan, R.; Zhu, Y.; You, L.; Wang, J.; Jin, X.; Zhang, Q.; Song, Y.; Chen, Z.; Li, Q. Integration of green $CuInS_2$/ZnS quantum dots for high-efficiency light-emitting diodes and high-responsivity photodetectors. *Opt. Mater. Express* **2018**, *8* (2), 314−323.
(35) Kim, J. H.; Jo, D. Y.; Lee, K. H.; Jang, E. P.; Han, C. Y.; Jo, J. H.; Yang, H. White Electroluminescent Lighting Device Based on a Single Quantum Dot Emitter. *Adv. Mater.* **2016**, *28* (25), 5093−5098.
(36) Bai, X.; Purcell-Milton, F.; Gun'ko, Y. K. Optical Properties, Synthesis, and Potential Applications of Cu-Based Ternary or Quaternary Anisotropic Quantum Dots, Polytypic Nanocrystals, and Core/Shell Heterostructures. *Nanomaterials* **2019**, *9* (1), 85−120.
(37) Omata, T.; Nose, K.; Otsuka-Yao-Matsuo, S. Size dependent optical band gap of ternary I-III-VI_2 semiconductor nanocrystals. *J. Appl. Phys.* **2009**, *105* (7), 073106−073111.
(38) Hamanaka, Y.; Ozawa, K.; Kuzuya, T. Enhancement of Donor−Acceptor Pair Emissions in Colloidal $AgInS_2$ Quantum Dots with High Concentrations of Defects. *J. Phys. Chem. C* **2014**, *118* (26), 14562−14568.
(39) Martynenko, I. V.; Baimuratov, A. S.; Weigert, F.; Soares, J. X.; Dhamo, L.; Nickl, P.; Doerfel, I.; Pauli, J.; Rukhlenko, I. D.; Baranov, A. V.; Resch-Genger, U. Photoluminescence of Ag-In-S/ZnS quantum dots: Excitation energy dependence and low-energy electronic structure. *Nano Research* **2019**, *12* (7), 1595−1603.
(40) Padmavathy, R.; Amudhavalli, A.; Rajeswarapalanichamy, R.; Iyakutti, K. Structural, electronic and mechanical properties of $AgIn_{1-X}Ga_XS_2$ (X = 0, 0.25, 0.50, 0.75, 1) chalcogenides. *Indian J. Phys.* **2021**, *95* (9), 1751−1756.
(41) Pu, C.; Qin, H.; Gao, Y.; Zhou, J.; Wang, P.; Peng, X. Synthetic Control of Exciton Behavior in Colloidal Quantum Dots. *J. Am. Chem. Soc.* **2017**, *139* (9), 3302−3311.
(42) Kobosko, S. M.; Kamat, P. V. Indium-Rich $AgInS_2$−ZnS Quantum Dots—Ag-/Zn-Dependent Photophysics and Photovoltaics. *J. Phys. Chem. C* **2018**, *122* (26), 14336−14344.
(43) You, Y.; Tong, X.; Imran Channa, A.; Zhi, H.; Cai, M.; Zhao, H.; Xia, L.; Liu, G.; Zhao, H.; Wang, Z. High-efficiency luminescent solar concentrators based on Composition-tunable Eco-friendly Core/shell quantum dots. *Chem. Eng. J.* **2023**, *452*, 139490−139496.
(44) Uematsu, T.; Tepakidareekul, M.; Hirano, T.; Torimoto, T.; Kuwabata, S. Facile High-Yield Synthesis of Ag−In−Ga−S Quaternary Quantum Dots and Coating with Gallium Sulfide Shells for Narrow Band-Edge Emission. *Chem. Mater.* **2023**, *35* (3), 1094−1106.
(45) Motomura, G.; Uematsu, T.; Kuwabata, S.; Kameyama, T.; Torimoto, T.; Tsuzuki, T. Quantum-Dot Light-Emitting Diodes Exhibiting Narrow-Spectrum Green Electroluminescence by Using Ag-In-Ga-S/GaS_x Quantum Dots. *ACS Appl. Mater. Interfaces* **2023**, *15* (6), 8336−8344.
(46) Li, Q.; Zheng, X.; Shen, X.; Ding, S.; Feng, H.; Wu, G.; Zhang, Y. Optimizing the Synthetic Conditions of "Green" Colloidal $AgBiS_2$ Nanocrystals Using a Low-Cost Sulfur Source. *Nanomaterials* **2022**, *12* (21), 3742−3751.
(47) Hoisang, W.; Uematsu, T.; Torimoto, T.; Kuwabata, S. Photoluminescence Stability Enhancement of Ag−In−Ga−S/GaS_x Core/Shell Quantum Dots with Thicker Shells by the Addition of Gallium Diethyldithiocarbamate. *Chem. Lett.* **2021**, *50* (11), 1863−1866.
(48) Wang, Z.; Zhang, X.; Xin, W.; Yao, D.; Liu, Y.; Zhang, L.; Liu, W.; Zhang, W.; Zheng, W.; Yang, B.; Zhang, H. Facile Synthesis of Cu−In−S/ZnS Core/Shell Quantum Dots in 1-Dodecanethiol for

https://doi.org/10.1021/acs.nanolett.2c03138
Nano Lett. XXXX, XXX, XXX−XXX

Efficient Light-Emitting Diodes with an External Quantum Efficiency of 7.8%. *Chem. Mater.* **2018**, *30* (24), 8939−8947.
(49) Zhang, Y.; Chang, C.; Liu, P.; Lei, J.; Cai, J. Ag_2S Nanoparticles Evolved into Luminescent $AgInS_2$@In_2S_3 Heteronanoparticles through Dual Formation Mechanism. *Part. Part. Syst. Char.* **2022**, *39* (7), 2200054−2200060.
(50) Kim, J.-H.; Lee, K.-H.; Jo, D.-Y.; Lee, Y.; Hwang, J. Y.; Yang, H. Cu−In−Ga−S quantum dot composition-dependent device performance of electrically driven light-emitting diodes. *Appl. Phys. Lett.* **2014**, *105* (13), 133104−133109.
(51) Bai, T.; Wang, X.; Dong, Y.; Xing, S.; Shi, Z.; Feng, S. One-Pot Synthesis of High-Quality $AgGaS_2$/ZnS-based Photoluminescent Nanocrystals with Widely Tunable Band Gap. *Inorg. Chem.* **2020**, *59* (9), 5975−5982.
(52) Mei, S.; Zhang, G.; Yang, W.; Wei, X.; Zhang, W.; Zhu, J.; Guo, R. A facile route for highly efficient color-tunable Cu-Ga-Se/ZnSe quantum dots. *Appl. Surf. Sci.* **2018**, *456*, 876−881.
(53) Kim, J.-H.; Kim, B.-Y.; Jang, E.-P.; Yoon, S.-Y.; Kim, K.-H.; Do, Y. R.; Yang, H. Synthesis of widely emission-tunable Ag−Ga−S and its quaternary derivative quantum dots. *Chem. Eng. J.* **2018**, *347*, 791−797.
(54) Rismaningsih, N.; Yamauchi, H.; Kameyama, T.; Yamamoto, T.; Morita, S.; Yukawa, H.; Uematsu, T.; Baba, Y.; Kuwabata, S.; Torimoto, T. Photoluminescence properties of quinary Ag−(In,Ga)−(S,Se) quantum dots with a gradient alloy structure for in vivo bioimaging. *J. Mater. Chem. C* **2021**, *9* (37), 12791−12801.
(55) Huang, G.; Huang, Y.; Liu, Z.; Wei, J.; Zhu, Q.; Jiang, G.; Jin, X.; Li, Q.; Li, F. White light-emitting diodes based on quaternary Ag−In-Ga-S quantum dots and their influences on melatonin suppression index. *J. Lumin.* **2021**, *233*, 117903−117911.
(56) Hoisang, W.; Uematsu, T.; Torimoto, T.; Kuwabata, S. Luminescent Quaternary $Ag(In_xGa_{1-x})S_2$/GaS_y Core/Shell Quantum Dots Prepared Using Dithiocarbamate Compounds and Photoluminescence Recovery via Post Treatment. *Inorg. Chem.* **2021**, *60* (17), 13101−13109.
(57) Thi Thu Huong, T.; Loan, N. T.; Ung, T. D. T.; Tung, N. T.; Han, H.; Liem, N. Q. Systematic synthesis of different-sized $AgInS_2$/GaS_x nanocrystals for emitting the strong and narrow excitonic luminescence. *Nanotechnology* **2022**, *33* (35), 355704−355712.
(58) Jo, D. Y.; Kim, D.; Kim, J. H.; Chae, H.; Seo, H. J.; Do, Y. R.; Yang, H. Tunable White Fluorescent Copper Gallium Sulfide Quantum Dots Enabled by Mn Doping. *ACS Appl. Mater. Interfaces* **2016**, *8* (19), 12291−12297.
(59) Huong, T. T. T.; Loan, N. T.; Van Long, L.; Phong, T. D.; Ung Thi Dieu, T.; Liem, N. Q. Highly luminescent air-stable $AgInS_2$/ZnS core/shell nanocrystals for grow lights. *Opt. Mater.* **2022**, *130*, 112564−112571.
(60) Ji, C.; Lu, M.; Wu, H.; Zhang, X.; Shen, X.; Wang, X.; Zhang, Y.; Wang, Y.; Yu, W. W. 1,2-Ethanedithiol Treatment for $AgIn_5S_8$/ZnS Quantum Dot Light-Emitting Diodes with High Brightness. *ACS Appl. Mater. Interfaces* **2017**, *9* (9), 8187−8193.
(61) Miropoltsev, M.; Kuznetsova, V.; Tkach, A.; Cherevkov, S.; Sokolova, A.; Osipova, V.; Gromova, Y.; Baranov, M.; Fedorov, A.; Gun'ko, Y.; Baranov, A. FRET-Based Analysis of $AgInS_2$/ZnAgInS/ZnS Quantum Dot Recombination Dynamics. *Nanomaterials* **2020**, *10* (12), 2455−2469.
(62) Fan, C. M.; Regulacio, M. D.; Ye, C.; Lim, S. H.; Zheng, Y.; Xu, Q. H.; Xu, A. W.; Han, M. Y. Colloidal synthesis and photocatalytic properties of orthorhombic $AgGaS_2$ nanocrystals. *Chem. Commun. (Camb.)* **2014**, *50* (54), 7128−7131.
(63) Jo, D.-Y.; Yang, H. Synthesis of highly white-fluorescent Cu−Ga−S quantum dots for solid-state lighting devices. *Chem. Commun.* **2016**, *52* (4), 709−712.
(64) Kim, J.-H.; Kim, B.-Y.; Yang, H. Synthesis of Mn-doped $CuGaS_2$ quantum dots and their application as single downconverters for high-color rendering solid-state lighting devices. *Opt. Mater. Express* **2018**, *8* (2), 221−230.
(65) Kim, J.-H.; Kim, B.-Y.; Jang, E.-P.; Han, C.-Y.; Jo, J.-H.; Do, Y. R.; Yang, H. A near-ideal color rendering white solid-state lighting device copackaged with two color-separated Cu−X−S (X = Ga, In) quantum dot emitters. *J. Mater. Chem. C* **2017**, *5* (27), 6755−6761.
(66) Kim, J.-H.; Yang, H. High-Efficiency Cu−In−S Quantum-Dot-Light-Emitting Device Exceeding 7%. *Chem. Mater.* **2016**, *28* (17), 6329−6335.
(67) Li, X.; Wu, Y.; Zhang, S.; Cai, B.; Gu, Y.; Song, J.; Zeng, H. $CsPbX_3$ Quantum Dots for Lighting and Displays: Room-Temperature Synthesis, Photoluminescence Superiorities, Underlying Origins and White Light-Emitting Diodes. *Adv. Funct. Mater.* **2016**, *26* (15), 2435−2445.
(68) Zeng, H.; Duan, G.; Li, Y.; Yang, S.; Xu, X.; Cai, W. Blue Luminescence of ZnO Nanoparticles Based on Non-Equilibrium Processes: Defect Origins and Emission Controls. *Adv. Funct. Mater.* **2010**, *20* (4), 561−572.
(69) Fang, T.; Wang, T.; Li, X.; Dong, Y.; Bai, S.; Song, J. Perovskite QLED with an external quantum efficiency of over 21% by modulating electronic transport. *Sci. Bull.* **2021**, *66* (1), 36−43.
(70) Chen, J.; Wang, J.; Xu, X.; Li, J.; Song, J.; Lan, S.; Liu, S.; Cai, B.; Han, B.; Precht, J. T.; Ginger, D.; Zeng, H. Efficient and bright white light-emitting diodes based on single-layer heterophase halide perovskites. *Nat. Photonics* **2021**, *15* (3), 238−244.
(71) Zhang, S.; Yan, Z.; Li, Y.; Chen, Z.; Zeng, H. Atomically thin arsenene and antimonene: semimetal-semiconductor and indirect-direct band-gap transitions. *Angew. Chem., Int. Ed.* **2015**, *54* (10), 3112−3115.
(72) Li, J.; Xu, L.; Wang, T.; Song, J.; Chen, J.; Xue, J.; Dong, Y.; Cai, B.; Shan, Q.; Han, B.; Zeng, H. 50-Fold EQE Improvement up to 6.27% of Solution-Processed All-Inorganic Perovskite $CsPbBr_3$ QLEDs via Surface Ligand Density Control. *Adv. Mater.* **2017**, *29* (5), 1603885−1603893.
(73) Kim, S.-K.; Kim, Y.-S. Charge carrier injection and transport in QLED layer with dynamic equilibrium of trapping/de-trapping carriers. *J. Appl. Phys.* **2019**, *126* (3), 035704−035713.

https://doi.org/10.1021/acs.nanolett.2c03138
Nano Lett. XXXX, XXX, XXX−XXX